7-2014

Langevin and Fokker-Planck Analyses of Inhibited Molecular Passing Processes Controlling Transport and Reactivity in Nanoporous Materials

Chi-Jen Wang
Iowa State University

David Ackerman
Iowa State University, ackerman@iastate.edu

Igor I. Slowing
Iowa State University, islowing@iastate.edu

James W. Evans
Iowa State University, evans@ameslab.gov

Langevin and Fokker-Planck Analyses of Inhibited Molecular Passing Processes Controlling Transport and Reactivity in Nanoporous Materials

Abstract
Inhibited passing of reactant and product molecules within the linear pores of nanoporous catalytic materials strongly reduces reactivity. The dependence of the passing propensity P on pore radius R is analyzed utilizing Langevin dynamics to account for solvent effects. We find that $P \sim (R-Rc)\sigma$, where passing is sterically blocked for $R \leq Rc$, with σ below the transition state theory value. Deeper insight comes from analysis of the corresponding high-dimensional Fokker-Planck equation, which facilitates an effective small-P approximation, and dimensional reduction enabling utilization of conformal mapping ideas. We analyze passing for spherical molecules and also assess the effect of rotational degrees of freedom for elongated molecules.

Disciplines
Applied Mathematics | Chemistry | Physics

Comments
This article is from *Physical Review Letters* 113 (2014): 038301, doi:10.1103/PhysRevLett.113.038301.
Posted with permission.

Langevin and Fokker-Planck Analyses of Inhibited Molecular Passing Processes Controlling Transport and Reactivity in Nanoporous Materials

Chi-Jen Wang,[1,2] David M. Ackerman,[1] Igor I. Slowing,[1,3] and James W. Evans[1,4]
[1]*Ames Laboratory-U.S. DOE, Iowa State University, Ames, Iowa 50011, USA*
[2]*Department of Mathematics, Iowa State University, Ames, Iowa 50011, USA*
[3]*Department of Chemistry, Iowa State University, Ames, Iowa 50011, USA*
[4]*Department of Physics and Astronomy, Iowa State University, Ames, Iowa 50011, USA*
(Received 10 May 2014; revised manuscript received 18 June 2014; published 14 July 2014)

Inhibited passing of reactant and product molecules within the linear pores of nanoporous catalytic materials strongly reduces reactivity. The dependence of the passing propensity P on pore radius R is analyzed utilizing Langevin dynamics to account for solvent effects. We find that $P \sim (R - R_c)^\sigma$, where passing is sterically blocked for $R \leq R_c$, with σ below the transition state theory value. Deeper insight comes from analysis of the corresponding high-dimensional Fokker-Planck equation, which facilitates an effective small-P approximation, and dimensional reduction enabling utilization of conformal mapping ideas. We analyze passing for spherical molecules and also assess the effect of rotational degrees of freedom for elongated molecules.

DOI: 10.1103/PhysRevLett.113.038301 PACS numbers: 82.75.Jn, 05.40.−a, 82.75.Qt, 83.10.Mj

Inhibited diffusive transport in nanoporous materials has been analyzed extensively given applications to separations, sequestration, and catalysis [1–7]. These materials include zeolites with pore diameters from $d_p = 0.5$–2 nm [4], and mesoporous silica nanoparticles (MSN) with $d_p \geq 2$ nm [8]. For catalysis, there is the strong suppression of reactivity in catalytically-active nanoporous materials upon reducing the pore diameter to approach the single-file diffusion (SFD) regime where reactant and product molecules cannot pass within pores [9]. SFD is readily achieved for zeolites since molecular dimensions are comparable to d_p (e.g., 0.4 nm for methane, 0.7 nm for neopentane) [4], and sometimes for MSN given that the effective d_p can be reduced below 2 nm due to functionalization and attachment of reactant species to the pore walls [10]. For conversion reactions with SFD, the reactant is localized near the pore openings, the pore interior being populated by product which cannot be readily extruded [9]. Examples include Pd-catalyzed neopentane conversion in zeolites [11], and aldol condensation in amine-functionalized MSN [10]. Catalytic polymerization in narrow pores is also strongly impacted by inhibited passing [12].

The subtle interplay between inhibited transport, as characterized by a suitable passing propensity P for reactants and products, and reaction can be conveniently described by spatially coarse-grained models. In these models, the pore is divided into cells with width $\sim$1 nm matching molecular dimensions [13–18]. Transport is described by hopping to adjacent empty cells at rate h_α for species α, and also by exchange of species α and β in adjacent cells with rate $1/2(h_\alpha + h_\beta)p_{\rm ex}$ [17–19]. The exchange probability $p_{\rm ex}$ reflects P, and $P = p_{\rm ex} = 0$ for SFD. These models, also incorporating suitably specified kinetics for adsorption-desorption at pore openings and for reaction, can be analyzed precisely via kinetic Monte Carlo simulation [14–18] or via a generalized hydrodynamic theory [17].

System-specific modeling requires reliable assessment of P which depends strongly on the size and shape of the molecules relative to the pore radius, $R = d_p/2$ [7]. P will vanish at a critical pore radius R_c, where passing is sterically blocked for rigid-pore and hard-core molecular interactions. Close to this threshold, molecules must misalign laterally on opposite sides of the pore in order to pass, and if elongated must align orientationally both with the pore axis and with each other. Passing propensity can be assessed by many-particle molecular dynamics studies tracking the order of particles inside narrow pores [20,21]. However, this approach becomes inefficient for small P. More effective is to focus on the passing of a specific pair of molecules. One such previous study utilized a transition state theory (TST) type approximation [19].

Here, we focus on passing of a pair of molecules using overdamped Langevin dynamics [22] to describe passing in liquid-phase systems in the presence of a solvent. For hard-core interactions and a rigid pore, we find that $P \sim (R - R_c)^\sigma$, as $R \to R_c$, but with σ is below the TST value. This sharp transition would be smeared for flexible pores [23] and soft molecular interactions. For a deeper understanding of this behavior, we also analyze the equivalent high-dimensional Fokker-Planck (diffusion) equation (FPE) [22]. This facilitates a simplified reformulation for small P, as well as dimensional reduction allowing utilization of conformal mapping concepts to elucidate σ values. We naturally first analyze the canonical case of rotationally symmetric molecules, both circles in a two-dimensional rectangular channel and spheres in

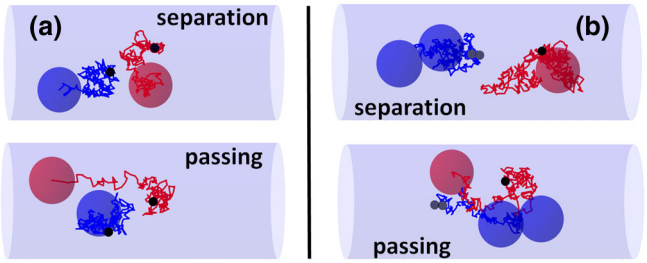

FIG. 1 (color online). Langevin trajectories for separating and passing events in a cylindrical pore with $g/r = 1$: (a) two spheres, $P = 0.116$; (b) sphere and dumbbell, $P = 0.066$. Small (large) circles indicate initial (final) configurations.

a three-dimensional cylindrical pore. The choice of a spherical geometry is common in modeling of transport of CH_3, CF_4, CCl_4, etc., [21] and reasonable for neopentane. We also consider behavior for elongated molecules with cylindrical symmetry, a description which has been applied for ethane [19], and which is reasonable for longer chain hydrocarbons and other oligomers.

We implement overdamped Langevin dynamics for a pair of molecules inside a pore which is aligned with the z axis. The analysis is formulated for possibly elongated molecules with cylindrical symmetry in thee dimensions and a nonzero moment of inertia $I_{||}$ orthogonal to the long axis. Such an elongated molecule has three translation degrees of freedom (d.o.f.) and two angular d.o.f.. It is convenient to implement incremental changes in coordinates in the body-fixed frame as follows. For changes in position parallel (x_1) and orthogonal ($x_{2,3}$) to the current orientation of the long axis, we assign translational drag coefficients $\zeta_1 = \zeta_{||}$ and $\zeta_{2,3} = \zeta_\perp$, drag forces $\mathrm{F}_i^{\mathrm{drag}} = -\zeta_i dx_i/dt$, and counterbalancing random forces $\mathrm{F}_i^{\mathrm{rnd}}(t)$. Then, denoting ensemble averages by $\langle\,\rangle$, one has

$$\zeta_i dx_i = \mathrm{F}_i^{\mathrm{rnd}}(t)dt, \quad \text{where } \langle F_i^{\mathrm{rnd}}(t)\rangle = 0 \quad \text{and}$$
$$\langle F_i^{\mathrm{rnd}}(t)F_j^{\mathrm{rnd}}(t')\rangle = 2k_BT\zeta_i\delta_{i,j}\delta(t-t'), \tag{1}$$

consistent with the fluctuation-dissipation relation [22] and diffusion coefficients $D_i = k_BT/\zeta_i$. For rotational dynamics, angles θ_i are conveniently selected as polar rotations about the long axis in two orthogonal planes. We similarly assign a rotational drag coefficient ζ_{rot}, drag torques $\tau_i^{\mathrm{drag}} = -\zeta_{\mathrm{rot}}d\theta_i/dt$, and counterbalancing random torques, $\tau_i^{\mathrm{rnd}}(t)$, so that $\zeta_{\mathrm{rot}}\, d\theta_i = \tau_i^{\mathrm{rnd}}(t)dt$ where $\langle\tau_i^{\mathrm{rnd}}(\mathrm{t})\rangle = 0$ and $\langle\tau_i^{\mathrm{rnd}}(t)\tau_j^{\mathrm{rnd}}(t')\rangle = 2k_BT\zeta_{\mathrm{rot}}\delta_{i,j}\delta(t-t')$. The rotational diffusion coefficient satisfies $\mathrm{D}_{\mathrm{rot}} = k_BT/\zeta_{\mathrm{rot}}$. After incremental motion, we accept the move only if it satisfies the nonoverlap conditions between the molecules themselves and the pore wall. The new coordinates are transformed back to a space-fixed frame to track absolute and relative molecular locations. There is an obvious reduction in the number of d.o.f. for benchmark analysis with molecules in two dimensions, and for rotationally symmetric molecules where $\zeta_{||} = \zeta_\perp$ and there is no angular motion. In the latter case, one can use a space-fixed frame with $x_1 = z$. Fig. 1 shows simulated trajectories for passing and separation events for two spheres, and for a sphere and a dumbbell-shaped diatomic of two joined spheres (where all spheres have equal radii) in a cylindrical pore.

Next, we describe the specific setup in our Langevin analysis of passing propensities P. Let δz denote the center-of-mass separation for the pair of molecules along the pore axis. It will be convenient to denote the various lateral center-of-mass coordinates and the orientations collectively denoted by $\underline{q}$. For molecule, α, let r_α denote the radius of a circumscribing sphere. We consider initial configurations where adjacent molecules, α and β, start with separation $\delta z = r_\alpha + r_\beta = d_{\alpha\beta}$. We select all other initial translational

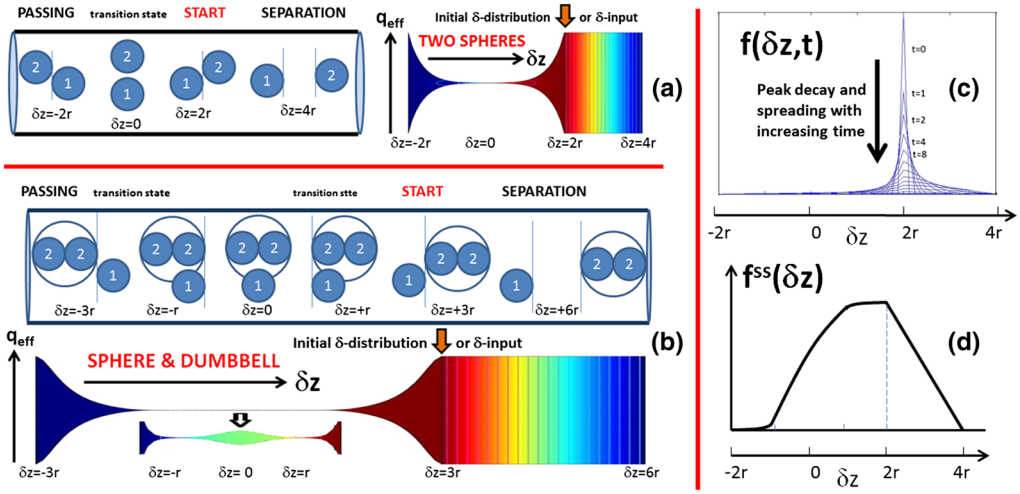

FIG. 2 (color online). Schematics of passing and separating configurations for (a) two spheres and (b) a sphere and dumbbell. Also shown: effective pore in $(\delta z, q_{\mathrm{eff}})$-phase space with $g/r = 1/8$ in (a), and $g/r = 1/32$ (expanded near $\delta z = 0$) in (b), and $f^{\mathrm{ss}}(\delta z, q_{\mathrm{eff}})$, where $f^{\mathrm{ss}} = 0$ at the ends is dark blue, and the maximum f^{ss} is dark maroon. Schematics of (c) $f(\delta z,t) = \int d\underline{q} f(\delta z,\underline{q};t)$ and (d) $f^{\mathrm{ss}}(\delta z) = \int d\underline{q} f^{\mathrm{ss}}(\delta z, \underline{q})$.

and rotational coordinates $\underline{q}$ randomly, subject to the constraint that the molecules are within the pore. We follow their evolution either until they separate (defined as reaching $\delta z = 2d_{\alpha\beta}$) or pass (defined as reaching $\delta z = -d_{\alpha\beta}$). See Figs. 2(a), 2(b). Note that in the initial and final configurations, there is no hindrance of rotation of one molecule by the other. This specification of passing is compatible with the coarse-grained models described above. From a large number N of simulation trials with $N_{\rm pass}$ passing outcomes, we obtain $P \approx N_{\rm pass}/N$. Note that $P_{\rm max} = 1/3$ for very wide pores where molecules do not interact, since δz changes by $-2d_{\alpha\beta}$ for passing, and only by $+d_{\alpha\beta}$ for separation. One can show that P is related to the parameter, $p_{\rm ex}$, in the coarse-grained models by $P = p_{\rm ex}/(2 + p_{\rm ex})$.

First, we present a detailed Langevin analysis of passing for canonical cases of equal-sized two-dimensional circular and three-dimensional spherical molecules of radius r. The critical pore radius is $R_c = 2r$. We introduce a gap size, $g = 2(R - R_c)$, and expect that $P \sim (g/r)^{\sigma}$, as $g \to 0$. The passing propensity P versus g is shown for circles in a two-dimensional rectangular channel [Fig. 3(a)], and spheres in a three-dimensional cylindrical pore [Fig. 3(b)]. P (spheres) exceeds P (circles) for g/r above $\sim$0.1 as expected from a simplified FPE analysis below. On the other hand, we find that $\sigma \approx 1.7$ for spheres, and $\sigma \approx 1.4$ for circles (also supported by FPE analysis). Thus, P (circles) dominates P (spheres), as $g \to 0$. Note that to obtain precise P values requires many simulation trials for small g (e.g., $N \sim 10^7$ for $g/r \sim 10^{-2}$), and a suitably small time step dt. P increases as $dt \to 0$, since very small steps aid negotiating narrow gaps. For $g/r < 0.1$, our P become imprecise even for our smallest $dt \sim 10^{-6}$ (natural dimensionless units). Second, we report P values for a sphere and dumbbell-shaped diatomic, where all spheres have radii r, and again

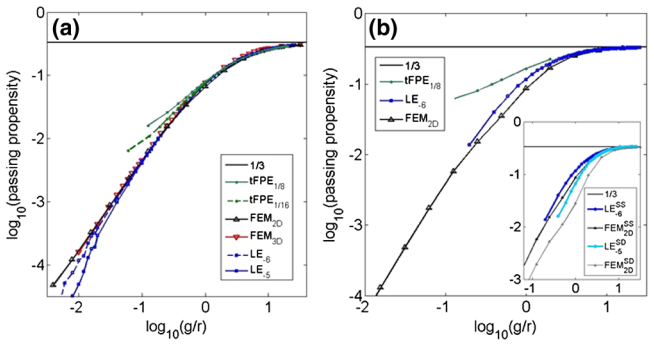

FIG. 3 (color online). P for (a) two circles in two dimensions: Langevin (LE) results (blue) for $dt = 10^{-5}$, 10^{-6} (dashed); time-dependent Fokker-Planck equation (tFPE) (green) for $r/8$, $r/16$ grids; full 3D FEM (red); effective two-dimensional FEM (black) and (b) two spheres in three dimensions: LE for $dt = 10^{-6}$ (blue); tFPE (green); effective two-dimensional FEM (red). Inset: P for two spheres (SS) versus a sphere + dumbbell (SD); LE and two-dimensional FEM (where FEM is final element method).

$R_c = 2r$. We select $D_{||} = 2$, $D_{\perp} = 1$ (in units of r^2 per unit time), and $D_{\rm rot} = 5$ (in radian^2 per unit time), although behavior should not depend strongly on specific O(1) values. Passing probabilities are lower than for two spheres (by a factor of $\sim$0.4 at $g/r < 0.5$), and our data suggest a similar exponent, $\sigma \approx 1.7$. See Fig. 3(b) (inset). We discuss this behavior further below. Precise determination of the true asymptotic σ is difficult (except in two dimensions), but one could argue that the readily determined effective σ value for $g/r \sim 0.1$–1 is of more practical importance.

Another instructive but approximate perspective on passing behavior comes from a TST type analysis of the free energy barrier to be surmounted during passing [19]. Let $V(\delta z)$ denote the accessible phase-space volume for lateral and rotational coordinates $\underline{q}$ for fixed δz. Then, in these models with just steric interactions, the free energy is purely entropic and the barrier for passing satisfies $\delta F = k_B T \ln[V_{\rm max}/V_{\rm min}]$, with $V_{\rm max} = V(|\delta z| > d_{\alpha\beta})$ and $V_{\rm min} = V(\delta z*)$, where $\delta z*$ is the transition state (TS) for passing. Thus, the TST passing probability scales like $P_{\rm TST} \sim \exp[-\delta F/(k_B T)] \sim V_{\rm min}/V_{\rm max}$. For two circular molecules in a rectangular channel, one has $\delta z* = 0$ and $P_{\rm TST} \sim V_{\rm min} \sim (g/r)^2$, as $g \to 0$ (i.e., $\sigma_{\rm TST} = 2$), since both molecules are confined to a distance $\sim g/r$ from the pore wall. For two spherical molecules in a cylindrical pore, orienting the configuration at $\delta z* = 0$ so that one molecule is on the vertical axis through the pore center, both molecules are confined to a distance of order g/r from the wall, and the center of the other molecule is confined to an angular range $\sim (g/r)^{1/2}$ from the vertical axis. Thus, one has that $P_{\rm TST} \sim V_{\rm min} \sim (g/r)^{2.5}$ as $g \to 0$ (i.e., $\sigma_{\rm TST} = 2.5$). The TS for the sphere-dumbbell system correspond to $\delta z* = \pm$r where one sphere of the dumbbell is aligned with the spherical molecule. Given the similarity to the TS for two spheres, one has again $\sigma_{\rm TST} = 2.5$. Below we elucidate the discrepancy between these $\sigma_{\rm TST}$ and lower Langevin estimates of σ.

Langevin dynamics can be analyzed by the equivalent time-dependent FPE, which for passing with steric blocking just corresponds to a high-dimensional diffusion equation [22,24]. One considers the probability, $f(\delta z, \underline{q}; t)$, of finding two molecules confined inside the pore with center-of-mass z-coordinate separation, δz, and for various lateral coordinates and orientations, $\underline{q}$. In our analysis of P, adjacent molecules start with $\delta z = d_{\alpha\beta}$, so that normalized $f(\delta z, \underline{q}; t = 0) = V(d_{\alpha\beta})^{-1}\delta(\delta z - d_{\alpha\beta})$. Since we follow evolution either until the molecules separate (reaching $\delta z = 2d_{\alpha\beta}$) or pass (reaching $\delta z = -d_{\alpha\beta}$), this corresponds to imposing adsorbing boundary conditions (BCs) $f = 0$ for these δz. We also impose zero-flux Neumann BCs at the boundary of the physically accessible region for other coordinates. The above constitutes a diffusion problem in a high-dimensional constricted channel. See Figs. 2(a), 2(b) for a two-dimensional representation. P is determined by accumulating over time the probability flux reaching

$\delta z = -d_{\alpha\beta}$ [see Fig. 2(c)]. Numerical analysis of this FPE initial value problem was performed using a hypercubic mesh in $(\delta z, \underline{q})$ space. As an aside, [25] analyzes $f(\delta z, t)$ for soft point-particles on a line where $\underline{q}$ is absent and steric effects cannot be assessed. Also, our FPE problem has some similarity with "narrow escape problems" considered in applied mathematics [26].

We find agreement of time-dependent FPE with Langevin results for larger g, but deviations for smaller g where accuracy is limited by finite mesh spacing. To resolve the computational challenges for small g, we consider an equivalent time-independent FPE formulation of the passing problem in which probability is continually fed into the system at $\delta z = d_{\alpha\beta}$ and absorbed at $\delta z = -d_{\alpha\beta}$ and $2d_{\alpha\beta}$ (see the Supplemental Material [24]). Now, P is obtained from the relative fluxes at $\delta z = -d_{\alpha\beta}$ and $2d_{\alpha\beta}$ as determined from the steady-state solution $f_{ss}(\delta z, \underline{q})$. There is a natural simplification for small g, where f_{ss} decreases linearly in δz for $\delta z > d_{\alpha\beta}$ to zero at $\delta z = 2d_{\alpha\beta}$. f_{ss} is roughly constant for $\delta z < d_{\alpha\beta}$, while $V(\delta z)$ remains substantial but drops dramatically for lower δz, where $V(\delta z)$ is small around $\delta z*$, and remains low approaching $\delta z = -d_{\alpha\beta}$. See Figs. 2(a), 2(b) and Fig. 2(d). Thus, P can be determined for small g from a conventional mixed boundary value problem (BVP) for the FPE with Dirichlet BC $f_{ss} = 0$ at $\delta z = -d_{\alpha\beta}$ and $f_{ss} =$ constant at $\delta z = d_{\alpha\beta}$, and Neumann BC on the other boundaries. This problem can be analyzed precisely with adaptive-mesh finite-element methods (FEM).

For passing of two circular molecules in a two-dimensional rectangular channel, a detailed comparison of different approaches for assessing P versus g/r is presented in Fig. 3(a). Precise results for smaller g/r are obtained from FEM analysis [27] of the mixed BVP (in a three-dimensional phase space with two lateral positions and δz) confirming our Langevin estimate $\sigma \approx 1.4$. FEM results smoothly connect to those from the time-dependent FPE analysis, which are accurate for $g/r > 0.4$. Thus, together, these approaches give an accurate FPE-based global characterization of behavior. Langevin equation results agree with this analysis down to $g/r \approx 0.1$ below which they become inaccurate. For passing of two spheres, FPE analysis involves a five-dimensional phase space and our time-dependent FPE analysis is only reliable for above $g/r \sim 3$. See Fig. 3(b). Also adaptive-mesh FEM methods are not readily implemented in five dimensions.

To assess and further elucidate small-g behavior, particularly for higher-dimensional problems, it is instructive to consider an effective reduced-dimensional FPE analysis of the passing process. It is natural to consider replacing all the variables $\underline{q}$ by a single effective variable, q_{eff}. Specifically, we consider a two-variable FPE problem in $(\delta z, q_{\text{eff}})$-space for a pore of width $V(\delta z)$ in the q_{eff} coordinate at position δz and with BCs analogous to the higher-dimensional FPE (see the Supplemental Material [24]). See Figs. 2(a), 2(b). FEM analysis of the passing propensity, P_{eff}, for the appropriate two-variable mixed BVP in the regime of small $V_{\min}$ (i.e., small gap) reveals that $P_{\text{eff}} \sim (V_{\min})^{\nu}$. The ν values can vary from as low as $\nu \approx 0.15$ for a slit, to $\nu \approx 0.25$ for a V-shaped obstruction with $V \sim V_{\min} + c|\delta z|$, to $\nu = 0.4$–0.5 for curved obstructions with $V \sim V_{\min} + c(\delta z)^2$, or $\nu = 0.59$–0.68 for $V \sim V_{\min} + c(\delta z)^4$, to unity (TST value) for a narrow straight channel. The key point is that the behavior of the passing propensity depends not just on the size at the smallest constriction in the effective pore, but on the entire shape of the constriction. This should be anticipated since the exact solution of the effective two-variable mixed BVP can be obtained by applying a conformal mapping to transform the constricted pore into a rectangular channel, a transformation which requires increasing dilation in the δz direction as the gap vanishes. The conformal mapping depends on the entire constriction shape.

How reliable is the effective two-variable FPE analysis? We must first evaluate $V(\delta z)$ for which we implement Monte Carlo integration (and also analytic calculation for simpler cases). Then, using this $V(\delta z)$ for the passing of two circular molecules in a rectangular channel, we obtain P_{eff} in almost perfect agreement with the full three-dimensional FEM analysis for small g, again supporting the assignment $\sigma \approx 1.4$. In fact, P_{eff} is only slightly below precise values determined by other methods for moderate g/r, a somewhat accidental agreement as our mixed BVP should not capture exact behavior. See Fig. 3(a). Using $V(\delta z)$ for the passing of two spheres in a cylindrical pore, we obtain P_{eff} for small g shown in Fig. 3(b), which is compatible with behavior reliably obtained by other methods for larger g/r. P_{eff} behavior also supports our assignment of $\sigma \approx 1.7$. Note that in this case, P_{eff} matches less well precise Langevin results for moderate g/r (as expected in general). Two other useful observations follow from our effective two-dimensional analysis. First, examining $V(\delta z)$ versus δz for moderate g/r around 1, it is clear that the effective channel is more constricted for two circles versus two spheres, explaining our observation that $P(\text{spheres}) > P(\text{circles})$ in this regime. Second, for both

TABLE I. TST (Langevin equation) scaling exponents in two dimensions and three dimensions. C, S, D, and E stand for circle, sphere, dumbbell, and ellipse (or ellipsoid), respectively.

	2D $C+C$	2D $C+D$	2D $C+E$	3D $S+S$	3D $S+D$	3D $S+E$
σ (σ_{TST})	2 (1.4)	2 (1.4)	3 (–)	2.5 (1.7)	2.5 (1.7)	4.5 (–)

circles and spheres, we find that the curvature of $V(\delta z)$ at the TS $\delta z = 0$ vanishes as $g \to 0$, suggesting that $P_{\text{eff}} \sim (\text{V}_{\text{min}})^{\nu}$ with $\nu \approx 0.6$–0.7. Since $V_{\text{min}} \sim (g/r)^p$, with $p = 2$ (2.5) for circles (spheres), this implies that $\sigma = p\nu \approx 1.36$ (1.70) for $\nu \approx 0.68$, compatible with observed scaling exponents from Langevin and higher-dimensional FPE analysis.

Finally, we discuss passing for other molecular shapes, specifically elongated molecules with cylindrical symmetry in three dimensions (or with reflection symmetry about the long axis in two dimensions). For an elliptical and a circular molecule in a two-dimensional rectangular channel, the additional angular d.o.f. for the ellipse (cf. a circle) has a range of order g/r for small gaps at the TS $\delta z* = 0$, so that $P_{\text{TST}} \sim (g/r)^3$. Similarly, for an ellipsoidal and spherical molecule in a three-dimensional cylindrical pore, there are two additional angular d.o.f. for the ellipsoid (cf., a sphere) each of which is restricted to a range of order g for small gaps at the transition state $\delta z* = 0$, so that $P_{\text{TST}} \sim (g/r)^{4.5}$. For a pair of elliptical or ellipsoidal molecules, additional rotational degrees of freedom will further increase σ_{TST}. We anticipate that actual exponents, σ, will be smaller than the TS theory predictions.

For elongated molecules, P values and specifically scaling as $g/r \to 0$, depends on molecular shape. To contrast the above behavior for convex shapes, consider the case of a spherical and dumbbell-shaped molecule in three dimensions as shown in Figs. 1(b) and 3(b) (inset). As noted in our TST discussion, the TS no longer occurs at $\delta z* = 0$, but rather at $\delta z* = \pm r$. See Fig. 2(b). For each of these TS, the range of dumbbell orientations does not vanish as $g \to 0$. Thus, behavior is similar to that at the TS for a pair of spherical molecules, as should be the scaling, i.e., $P_{\text{TST}} \sim (g/r)^{2.5}$ versus $P \sim (g/r)^{1.7}$. The same should apply for a sphere passing an oligomer modeled as a chain of spheres. From a simple effective two-dimensional FEM analysis [see Fig. 3(b)] again obtaining $V(\delta z)$ from Monte Carlo integration, we obtain a reduction by a factor of 0.33 at $g/r = 0.4$ in P for the sphere-dumbbell versus two spheres, not so far from the Langevin estimate of 0.40 given that g/r is not small. Also, the two-dimensional FEM results for small g/r seem to be compatible with extrapolated LE results.

In summary, we have provided a general picture for the behavior of molecular passing processes in narrow pores controlled by Langevin dynamics, including scaling for small gap sizes. This scaling, as summarized in Table I, is not described by a simple TST, but rather depends on more global features of the confined geometry during the passing process.

This work was supported by the U.S. DOE-BES Division of Chemical Sciences, Geosciences, and Biosciences through the Chemical Physics program at Ames Laboratory (operated for the U.S. DOE by ISU under Contract No. DE-AC02-07CH11358).

[1] K. Malek, T. J. H. Vlugt, and B. Smit, in *Catalysis and Materials Science*, edited by R. A. van Santen and P. Sautet (Wiley, New York, 2009), Chap. 14.
[2] J. Kärger, in *Handbook on Heterogenous Catalysis*, edited by G. Ertl, H. Knözinger, F. Schüth, and J. Weitkamp (Wiley, New York, 2008), p. 1714.
[3] D. S. Sholl, Acc. Chem. Res. **39**, 403 (2006).
[4] N. Y. Chen, J. T. F. Degnan, and C. M. Smith, *Molecular Transport and Reaction in Zeolites* (VCH, New York, 1994).
[5] L. Heinke, D. Tzoulaki, C. Chmelik, F. Hibbe, J. M. van Baten, H. Lim, J. Li, R. Krishna, and J. Kärger, Phys. Rev. Lett. **102**, 065901 (2009).
[6] E. Beerdsen, D. Dubbeldam, and B. Smit, Phys. Rev. Lett. **96**, 044501 (2006).
[7] K. Hahn, J. Kärger, and V. Kukla, Phys. Rev. Lett. **76**, 2762 (1996).
[8] J. S. Beck, J. C. Vartulli, W. J. Roth, M. E. Leonowicz, C. T. Kresge, K. D. Schmitt, C. T. W. Chu, D. H. Olson, and E. W. Sheppard, J. Am. Chem. Soc. **114**, 10834 (1992).
[9] C. Rödenbeck, J. Kärger, and K. Hahn, J. Catal. **157**, 656 (1995).
[10] K. Kandel, S. M. Althaus, C. Peeraphatdit, T. Kobayashi, B. G. Trewyn, M. Pruski, and I. I. Slowing, J. Catal. **291**, 63 (2012).
[11] Z. Karpinski, S. N. Gandhi, and W. M. H. Sachtler, J. Catal. **141**, 337 (1993).
[12] D.-J. Liu, H.-T. Chen, V. S.-Y. Lin, and J. W. Evans, J. Chem. Phys. **132**, 154102 (2010).
[13] J. G. Tsikoyiannis and J. Wei, Chem. Eng. Sci. **46**, 233 (1991).
[14] C. Rödenbeck, J. Kärger, and K. Hahn, Phys. Rev. E **55**, 5697 (1997).
[15] M. S. Okino, R. Q. Snurr, H. H. Kung, J. E. Ochs, and M. L. Mavrovouniotis, J. Chem. Phys. **111**, 2210 (1999).
[16] S. V. Nedea, A. P. J. Jansen, J. J. Lukkien, and P. A. J. Hilbers, Phys. Rev. E **65**, 066701 (2002).
[17] D. M. Ackerman, J. Wang, and J. W. Evans, Phys. Rev. Lett. **108**, 228301 (2012).
[18] J. Wang, D. M. Ackerman, V. S.-Y. Lin, M. Pruski, and J. W. Evans, J. Chem. Phys. **138**, 134705 (2013).
[19] D. S. Sholl, Chem. Eng. J. (London) **74**, 25 (1999).
[20] D. Keffer, A. V. McCormick, and H. T. Davis, Mol. Phys. **87**, 367 (1996).
[21] D. S. Sholl and K. A. Fichthorn, J. Chem. Phys. **107**, 4384 (1997).
[22] W. T. Coffey, Yu. P. Kalmykov, and J. T. Waldron, *The Langevin Equation* (World Scientific, Singapore, 2004).
[23] R. V. Awati, P. I. Ravikovitch, and D. S. Sholl, J. Phys. Chem. C **117**, 13462 (2013); S. Jakobtorweihen, C. P. Lowe, F. J. Keil, and B. Smit, J. Chem. Phys. **124**, 154706 (2006).
[24] See the Supplemental Material at http://link.aps.org/supplemental/10.1103/PhysRevLett.113.038301 for further description of the FPE formulation.
[25] T. Ambjorsson and R. J. Silbey, J. Chem. Phys. **129**, 165103 (2008).
[26] D. Holcman and Z. Schuss, SIAM Rev. **56**, 213 (2014).
[27] COMSOL multiphysics adaptive-mesh FEM analysis (www.comsol.com).